Molecular-Level Modeling of the Structure and Wetting of Electrode/Electrolyte Interfaces in Hydrogen Fuel Cells

Junwu Liu,[†] Myvizhi Esai Selvan,[†] Shengting Cui,[†] Brian J. Edwards,[†] David J. Keffer,*[,†] and William V. Steele[†,‡]

Department of Chemical and Biomolecular Engineering, University of Tennessee, Knoxville, Tennessee 37996-2200, and Nuclear Science and Technology Division, Oak Ridge National Laboratory, Oak Ridge, Tennessee 37831-6273

Received: July 17, 2007; In Final Form: October 24, 2007

Molecular dynamics (MD) simulations were performed to investigate the structural and dynamical behavior of water and hydronium ions at the electrode/electrolyte interface of hydrogen polymer electrolyte membrane (PEM) fuel cells. Specifically, we have studied the hydrated Nafion membrane, humidified for four different water contents, 5, 10, 15, and 20%, at 300 K. We analyzed the three-phase interface where the hydrated PEM is in contact with the vapor phase and with either the catalyst surface (platinum in this paper) or the catalyst−support surface (graphite in this paper). These molecular simulations represent portions of interfaces that exist within the PEM fuel cells. We observed significant wetting of the catalyst surface by a mixture of polymer, water, and hydronium ions but not beyond a monolayer. We observed virtually no wetting of the graphite surface. On the catalyst surface, the degree of wetting of the catalyst surface depends strongly on the level of membrane humidity. The pair correlation functions indicate that the water molecules adsorbed in a monolayer on the catalyst surface form small domains of ordered structures, which are bound by fragments of Nafion on the surface. The diffusion of protons from the catalyst surface into the membrane must proceed across this highly inhomogeneous surface.

I. Introduction

A better understanding of the properties of the electrode/electrolyte interface is of practical significance in catalysis, proton transport, water electrolysis, and electrode coatings of polymer electrolyte membrane (PEM) fuel cells, which constitute a promising renewable energy source for automobile applications and portable devices such as cell phones and laptop computers. Essentially, a PEM fuel cell is composed of an anode, where hydrogen is electro-oxidized, a cathode, where oxygen is electroreduced, and a perfluorinated polymer electrolyte membrane, which serves as a structural framework and transports protons from anode to cathode. The study of the molecular level structure and of the dynamics at the interface between electrode and electrolyte offers new insights into the theory and mechanisms that control the electrochemical and electrocatalytic surface processes.

In recent years, many significant experiments,[1−21] classical molecular dynamics simulations (MD),[22−26,] and molecular-level simulations[27−30] have been conducted in attempts to understand the structural and dynamical properties of proton transport in the hydrated membrane. Key to the understanding of proton transport in hydrated Nafion is the understanding that hydrated Nafion is composed of two nanophases—a hydrophobic phase composed of the backbone of the Nafion and an aqueous phase composed of the water molecules, the hydronium ions, and the sulfonic acid groups at the end of the Nafion side chains. Proton transport occurs through the aqueous nanophase. Numerous idealized models of the morphology of the aqueous phase have been previously presented.[4,5,9]

More recently, classical MD simulations have been performed to understand the morphology of the aqueous nanophase in Nafion in different solvents, such as water and methanol. Vishnyakov and Neimark,[31] for example, found that water does not form a continuous subphase but forms isolated clusters of about 100 molecules in size. They also concluded that the clusters are connected through short-lived bridges instead of a continuous hydrophilic subphase. By comparison, Urata et al.[32] studied the water clustering and concluded that, in the short-range distance within 4.6−7.7 Å, a continuous aqueous phase bridged the sulfonic acid groups. Cui et al.[33] demonstrated through analyses of the water cluster size distributions that the vast majority of water molecules form a single, sample-spanning cluster of water contents at 15 and 20 wt %; however, as the humidity level is decreased, smaller, disconnected clusters are formed. The morphology of the aqueous nanophase can fluctuate in time.

Although much effort has been expended on the molecular-level characterization of proton transport in the hydrated membrane, substantially less work has concentrated on the atomic and molecular-level details of proton transport at the three-phase interface composed of the polymer electrolyte membrane, vapor, and catalyst surface. The electrochemical and electrocatalytic processes occurred at this interface ultimately dictate the overall performance of PEM fuel cells. In aqueous solution, a combination of experiment and simulation has led to a relatively clear molecular-level picture of water close to a Pt electrode.[34,35] Rossmeisl et al. used ab initio density functional theory to calculate the phase diagram for the oxidation and

* To whom correspondence should be addressed. E-mail: dkeffer@utk.edu.
[†] University of Tennessee.
[‡] Oak Ridge National Laboratory.

10.1021/jp075612l CCC: $40.75
Published on Web 01/23/2008

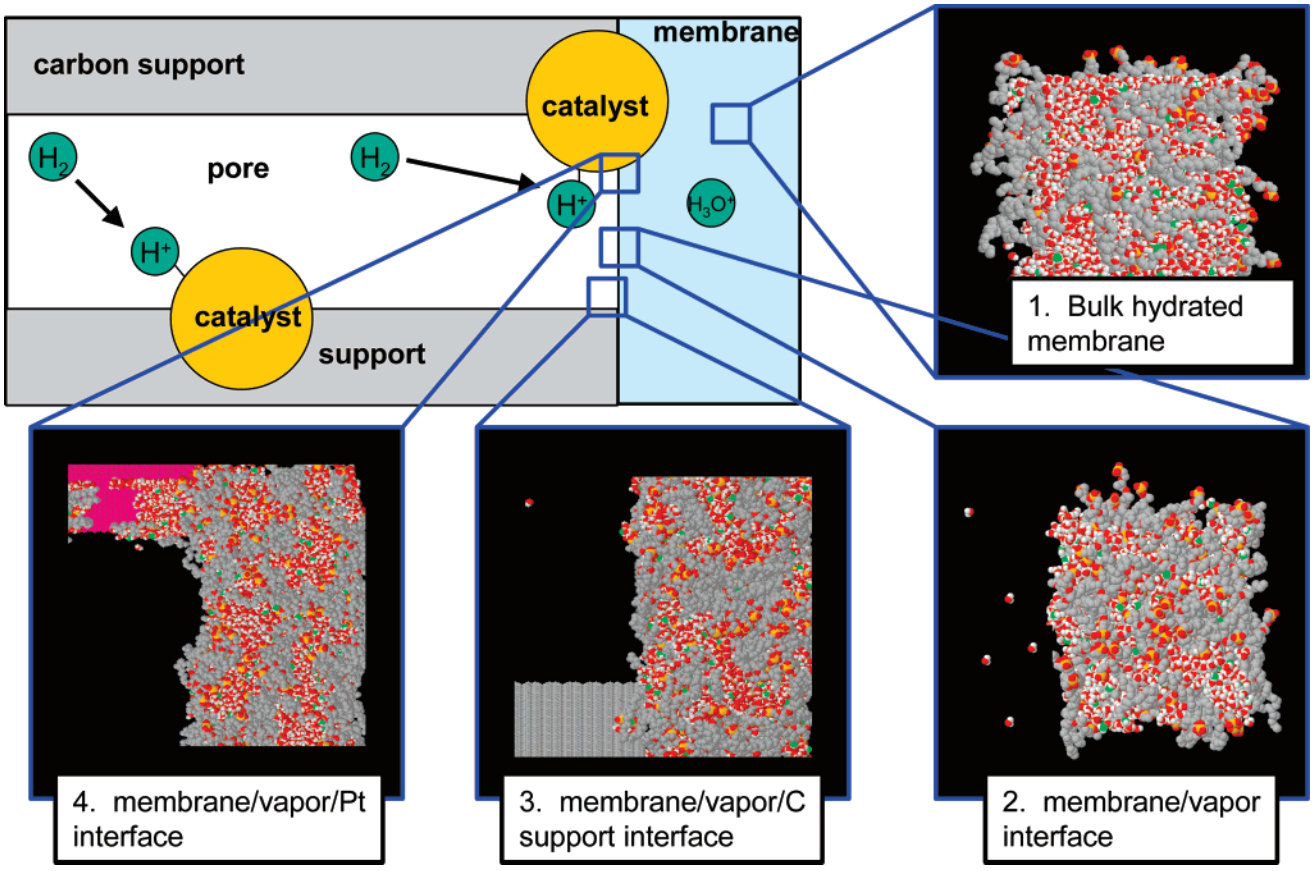

Figure 1. A schematic of the molecular-level interfaces present at the electrode/electrolyte interface of the anode of a PEM fuel cell.

reduction of water over Pt(111) surface.[36] However, this body of work models the electrode in aqueous solution without Nafion present.

One difficulty in modeling the three-phase hydrated PEM/catalyst/vapor interface is the possible variation in structure due to the manufacturing process and composition of the catalyst zone in the membrane electrode assembly (MEA). The performance of the fuel cell depends upon both the amount of ionomer introduced into the MEA as well as the manner in which was introduced.[37] For example, by use of gas chromatography and scanning electron microscopy (SEM) to study a Pt/C catalyst impregnated with a solution of Nafion, Broka and Ekdunge report that "it is more likely Pt agglomerates are only partially covered by Nafion".[38] By use of SEM and transmission electron microscopy (TEM) to study thin-film catalyst layers made by mixing the Pt/C catalyst with a Nafion solution, Cheng et al. report that low Pt catalyst utilization can result from catalyst particles being covered by "thick Nafion layers or clumps".[39] Various groups have varied the Nafion loading in the gas diffusion layer and found an optimum, reflecting the balance between enhanced proton conductivity and hindered gas diffusion at high Nafion content.[40,41]

By use of molecular simulation, Lamas et al.[42] formulated a model of the three-phase interface to investigate how the configurational and dynamic properties of water in the vicinity of the catalyst surface change with Nafion content. They also reported that the water dynamics adjacent to the catalyst surface vary significantly, according to the degree of membrane hydration.

In this work, we choose to focus on a MEA in which the catalyst surface is not completely covered by Nafion. In Figure 1, we present an idealized schematic of the model interface that is used as a basis for the molecular dynamics simulations reported herein. The schematic shows a single unit of the porous electrode. Catalyst particles are distributed on the surface of the pore, and the pore is in contact with the PEM. The specific geometry of this highly idealized schematic is not essential, and the schematic is not necessarily drawn to scale, which depends upon the pore size distribution of the electrode; however, the schematic illustrates the specific molecular-level interfaces that are present at the composite electrode/electrolyte interface. Specifically, four systems are isolated. The first system is the "bulk" hydrated membrane, which has been studied extensively via molecular dynamics.[23,31−33,43−47] The second system is the interface between the hydrated membrane and the vapor phase. The structure and dynamics of this system were recently reported using MD simulations.[48] The third system is the three-phase interface between the hydrated membrane, the vapor, and the surface of the catalyst support. The fourth system is the three-phase interface between the hydrated membrane, the vapor, and the surface of the catalyst particle. In this work, we report on the structure and dynamics of the third and fourth interfaces, which include the solid surfaces.

The molecular-level environment at the interface is also a function of operating conditions. The temperature and the humidity in the feed stream affect the amount of water in the pore. Under some conditions, the pore can be filled with water, which could completely cover the catalyst particle surface. In this situation, the diffusion of molecular hydrogen to the surface of the catalyst would be dramatically reduced. (At room temperature and pressure, the self-diffusivity of H_2 is 5.6×10^{-1} cm^2/s[49], and the diffusivity of H_2 in water is 4.5×10^{-5} cm^2/s.[50]) The increase in mass transfer resistance would be detrimental. However, the catalyst particle would then not require close contact to the PEM, since the hydronium ion could be transported through the aqueous phase.

In this present work, we are specifically examining the three-phase interface. Therefore, we choose to begin with a bare surface and will allow the PEM to relax over it, with the assumption that we are able to maintain a gas phase in the pore. Experimental adsorption isotherms of Nafion indicate that Nafion can be hydrated up to 20 wt % water (the highest loading studied here) through equilibrium with a vapor phase.[51]

We present the results of molecular dynamics simulations of hydrated Nafion at four different water contents by weight (5, 10, 15, and 20 wt %) in simultaneous contact with the vapor phase and either the catalyst surface or the catalyst support surface. The catalyst surface is modeled as a [100] Pt surface. The catalyst support surface is modeled as graphite.

The remainder of this paper is organized as follows. In section II, we briefly describe the methodology and summarize the computational details. The results of the molecular simulations are presented in section III. In section IV, we provide a discussion of the implications and conclusions of this simulation work on the molecular-level understanding of proton transport in fuel cells.

II. Simulation Details and Methodology

Two groups of NVT simulations were carried out at 300 K in this work. The first group of simulations was for the membrane/vapor/support system (system 3 in Figure 1). The second group of simulations was for the membrane/vapor/catalyst system (system 4 in Figure 1). Each group was composed of four simulations that were performed at varying water contents of 5, 10, 15, and 20 wt %. These weight percents correspond to ratios of H_2O/SO_3^- of 3.44, 5.42, 8.63, and 11.83., respectively.

The model of Nafion, water, and the hydronium ions used in this work is identical to that of our previous work to model bulk hydrated Nafion;[33] that is, each Nafion oligomer is a trimer. The short chain length is a compromise, owing to the fact that long chains have long relaxation times that are beyond the capacity of the simulations. We have previously shown that this model yields consistent results with Nafion chains composed of ten monomers.[33] Philosophically, one has to make a choice between modeling a system with long chains, in which one will not be able to run a simulation of sufficient duration to average out fluctuations due to chain dynamics, or a system with short chains in which the model is more approximate but the resulting statistics are much better.

For Nafion, we used united atoms for CF_3, CF_2, and CF to reduce computational costs. We included bond stretching, bending, torsion, and intramolecular and intermolecular non-bonded interactions via the Lennard-Jones (LJ) potential and Coulombic interactions. The potential parameters have been reported previously[52] and are taken from ref 53.

The water is modeled using the TIP3P model[54,55] with a flexible OH bond.[56] The model for hydronium ions, H_3O^+, is similar to that of Urata et al.[32] In particular, the partial charges for the oxygen and hydrogen atoms are taken from Urata et al.[32] The bond distance, bond angles, and force constants are the same as in the TIP3P model.[54−56] Note that this potential does not allow for structural diffusion of the proton. However, we believe that this nonreactive potential is capable of providing realistic static properties, such as configurations, as discussed previously.[33]

We modeled the surface of the support phase as graphite, in which the carbon atoms are held rigid and interact with all dynamic atoms in the system through the LJ potential with parameters $\sigma_C = 3.4$ Å and $\epsilon_C/k = 28.0$ K.[57] The positions of the graphite atoms are taken from the literature.[58] The graphite surface is four atomic layers deep.

TABLE 1: Size of the Three Dimensions of the Simulation Cell for Graphite/Platinum Systems (All Units Are in Angstroms)

	graphite			platinum		
water content	*x*	*y*	*z*	*x*	*y*	*z*
5 wt %	115.02	136.10	103.32	113.59	129.82	109.68
10 wt %	119.28	123.09	118.08	117.51	125.55	117.51
15 wt %	119.28	133.70	118.08	121.43	131.97	117.51
20 wt %	123.54	139.35	118.08	125.34	129.38	125.34

TABLE 2: Summary of the Simulation Conditions

	5 wt %	10 wt %	15 wt %	20 wt %
no. of polymers	256	256	256	256
no. of water molecules	2640	4160	6624	9088
no. of hydronium ions	768	768	768	768
total no. of particles	31728	36288	43680	51072
λ (H_2O/SO_3^-)	3.44	5.42	8.63	11.83
simulation time (ns)	4.0	4.0	4.0	4.0
no. of graphite atoms	3024	3584	3584	3712
no. of Pt atoms	4872	5400	5580	6144

We modeled the surface of the catalyst phase as [100] platinum, in which the atoms are held rigid and interact with all dynamic atoms in the system through the LJ potential with parameters $\sigma_{Pt} = 2.41$ Å and $\epsilon_{Pt}/k = 2336.0$ K.[59] The positions of the Pt atoms are taken from the literature.[60] The Pt surface is six atomic layers deep.

For all interactions, the LJ parameters for cross components were calculated using Lorentz−Berthelot mixing rules. The site−site reaction field was applied for the calculation of the electrostatic interactions.[61,62] Partial charges for united atom groups were calculated from the summations of the constituent atom values. The backbone was treated as neutral, except for the site to which the side chain is connected through the ether oxygen.

The amount of hydrated membrane material used for these interfacial systems is four times larger than that of our previous bulk hydrated membrane system,[33] in order to obtain better interfacial statistics. The size of the current simulation cell is nominally eight times that of the previous bulk hydrated membrane system size, with roughly half of the cell being occupied by the vapor phase, as was done in our strictly membrane/vapor systems.[48] The dimensions of each system are provided in Table 1. The dimensions of the solid surface in the *z* direction are nominally 60 Å. The dimensions of the cells change to accommodate the integer number of unit cell dimensions of the catalyst or support surface. The number of each type of molecule used in the simulation is provided in Table 2.

The initial conditions of the systems took an equilibrated bulk hydrated membrane from our previous work[33] and placed it next to a vacuum. Because the dimensions of the simulation cell varied according to the integer number of unit cells of catalyst or support surface present, there was a period in which the equilibrated membrane was gradually relaxed into the new aspect ratio of the cell, while maintaining a constant total simulation volume. The solid surface was artificially "grown" into the system gradually over a period of 10 ps to avoid overlap with the molecules in the hydrated membrane.

With the solid surface in place, we allow the full system to equilibrate. The water redistributes between the vapor, PEM, and solid surface. Thus, it is important to note that the nominal

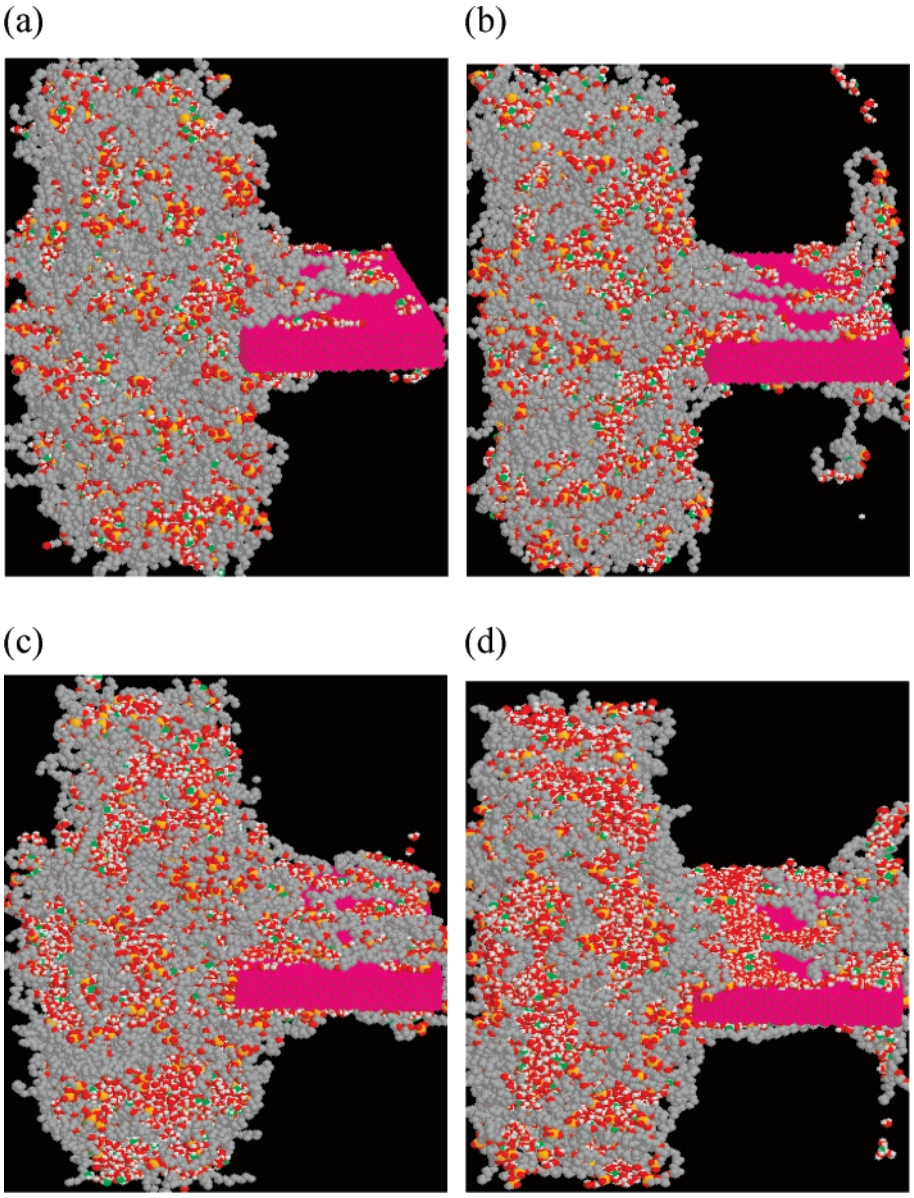

Figure 2. Final snapshots of simulations containing the catalyst surface for water contents of (a) 5, (b) 10, (c) 15, and (d) 20 wt %. The coloring legend is as follows: CF_x groups are gray; sulfur, orange; oxygen of H_2O and SO_3^-, red; oxygen of H_3O^+, green; hydrogen, white; platinum, pink.

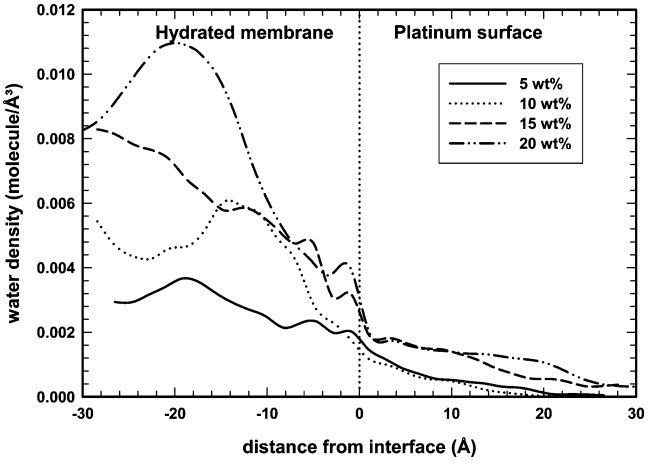

Figure 3. Density profile of water molecules along the *z* direction in the simulation cell for the catalyst system.

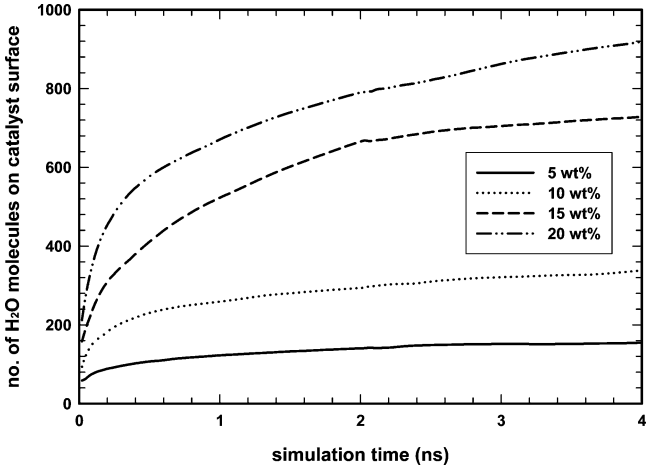

Figure 4. Wetting of the catalyst surface:number of water molecules on the catalyst surface as a function of time.

water contents reported in this work are the initial values of the hydrated membrane. This water content will decrease as the water leaves the membrane and enters the vapor phase or adsorbs to the solid phase.

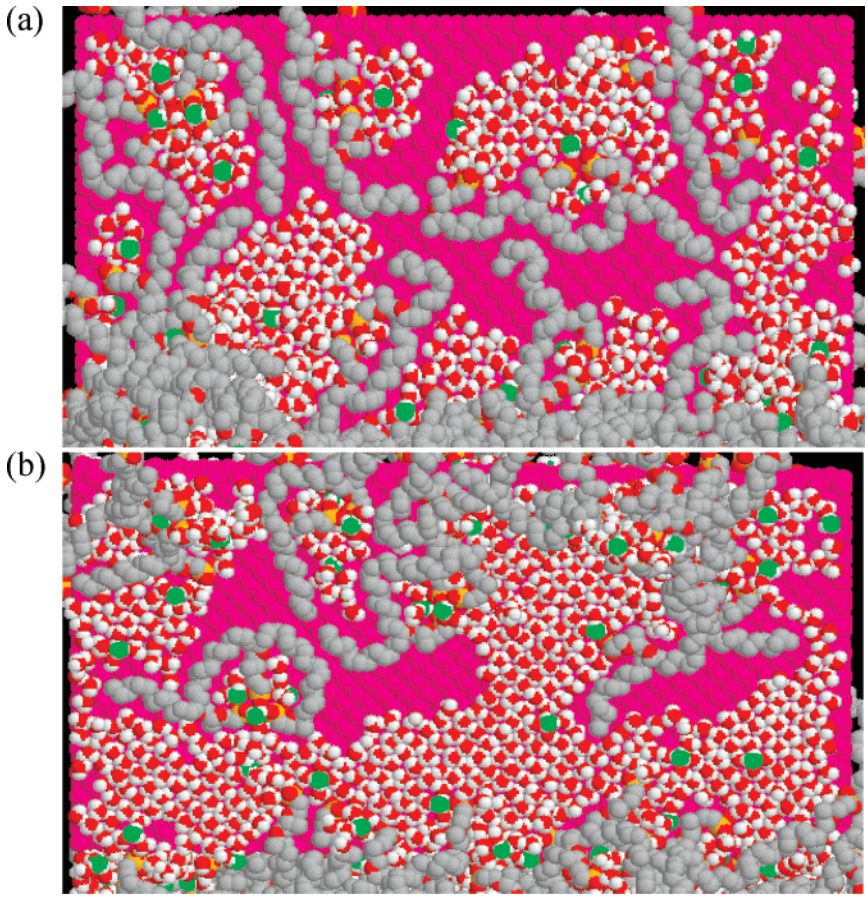

Figure 5. Final snapshot normal to the surface of simulations containing the catalyst for water contents of (a) 15 and (b) 20 wt %. The coloring legend is the same as Figure 2.

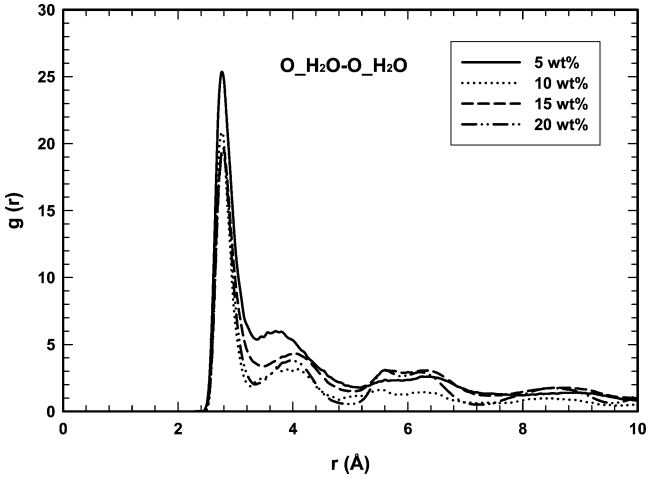

Figure 6. The pair correlation function for the oxygen atom of a water molecule with other oxygen atoms of water molecules (the $O_{H_2O}-O_{H_2O}$ PCF) in the adsorbed region next to the catalyst surface as a function of water content.

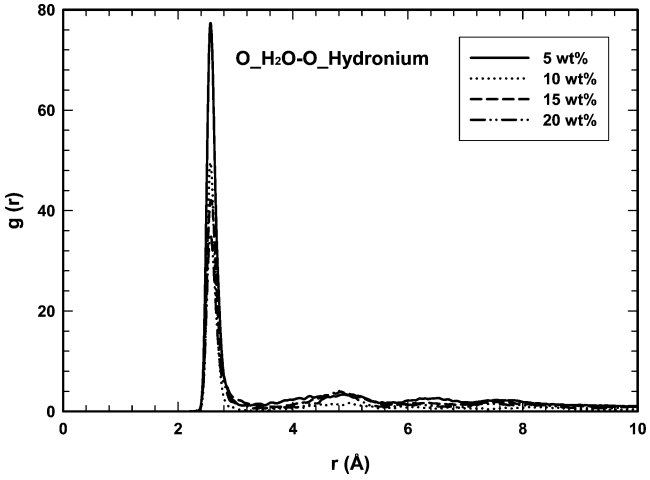

Figure 7. The pair correlation function for the oxygen atoms of water with oxygen atoms of hydronium ions (the $O_{H_2O}-O_{H_3O^+}$ PCF) in the adsorbed region next to the catalyst surface as a function of water content.

The simulations were equilibrated for 2 ns. The data production mode followed for an additional 2 ns. We employed the Nosé−Hoover thermostat,[63−65] and the r-RESPA method[66] was carried out to integrate the equations of motion with 2 fs for the large time step size and 0.2 fs for the intramolecular motions.

III. Results and Discussion

III.A. Membrane/Vapor/Catalyst Systems. In parts a−d of Figure 2, we present snapshots of the final configurations of the membrane/vapor/catalyst systems for hydrated membranes with initial water contents of 5, 10, 15, and 20 wt %, respectively. There are two surfaces visible because the simulations are periodic. However, the size of the system has been chosen to be large enough so that there were no artifacts associated with the periodicity. These snapshots clearly reveal that there is significant wetting of the platinum surface and that the degree of wetting increases with the water content. The snapshots also show that some fragments of Nafion as well as hydronium ions adsorb on the Pt surface. The fundamental reason for the adsorption of water, Nafion, and hydronium is the large attractive interaction due to the induced-dipole/induced-

dipole term of the LJ potential. At all water contents, we do not observe multilayer adsorption, except immediately adjacent to the membrane interface. At higher water contents, the adsorption approaches a complete monolayer of coverage.

The density profile of water in the catalyst system is shown in Figure 3. The zero coordinate on the *x* axis corresponds to the central location of the membrane/vapor interface. The variation of water density within the interface is a consequence of the fact that the nanostructured segregation of the hydrated membrane into hydrophobic and hydrophilic regions is not uniform on the nanoscale and also relaxes on a time scale that is greater than the duration of these simulations, as noted before.[33] However, there are several notable features in this plot. First, there is clearly a "dehydrated region" of the membrane near the interface. We observed this dehydration of the interface in the membrane/vapor simulations as well, so we conclude that this is an equilibrium state and is not a transient effect resulting from the catalyst surface extracting water from the membrane interface faster than it can be replenished from the membrane interior. Second, we observe only a monolayer density of water on the catalyst surface.

In these simulations, water is being drawn out of the hydrated Nafion in order to establish an equilibrium between the PEM, the vapor phase, and the adsorbed phase. In the vapor phase, we never observe any molecules but water. In other words, as one would naturally expect, there is no hydronium ion or Nafion in the vapor phase. Therefore, we understand that any hydronium or Nafion that appears on the catalyst surface reached the catalyst via surface diffusion. The water can travel to the catalyst surface by moving along the surface or by moving through the vapor phase. The net flux of water from membrane to surface via the vapor phase is much lower than that through surface diffusion. In these simulations, therefore, virtually all of the material on the catalyst arrived via surface diffusion.

The dynamics of wetting are shown in Figure 4, which shows the quantitative degree of wetting of the catalyst surface as a function of simulation time up to 4 ns. From these curves, it appears that, at lower water contents, the system has equilibrated, with the surface of the catalyst only partially covered by a mixture of water, Nafion, and hydronium ions. At high water contents, the wetting curves in Figure 4 still have a significant slope and are gradually continuing to increase in time. At 15 and 20 wt %, the snapshots indicate that there is already a continuous wet path across the catalyst surface. It is likely that in this simulation the surface would be completely wet, if we continued the simulations for a longer duration. We have not continued the simulations because the rate of additional wetting is slow relative to the duration of the simulations.

The reason for the deceleration in the rate of wetting can be partially attributed to a stable structure that forms on the catalyst surface. In Figure 5, we show the same snapshots shown in parts c and d of Figure 2 (15 and 20 wt %, respectively) from an angle normal to the catalyst surface. Here we see the regular structure that the water has formed on the surface. This structure optimizes the degree of hydrogen bonding in a two-dimensional array of water molecules. We observe that each water molecule has four nearest neighbors when the structure is stable. The monolayer coverage of the platinum surface suggests that the wetting of the surface is predominantly through direct transfer of water molecules from the membrane phase to the catalyst surface not through the vapor phase adsorption. Thus the direct contact between the membrane materials and the catalyst is important.

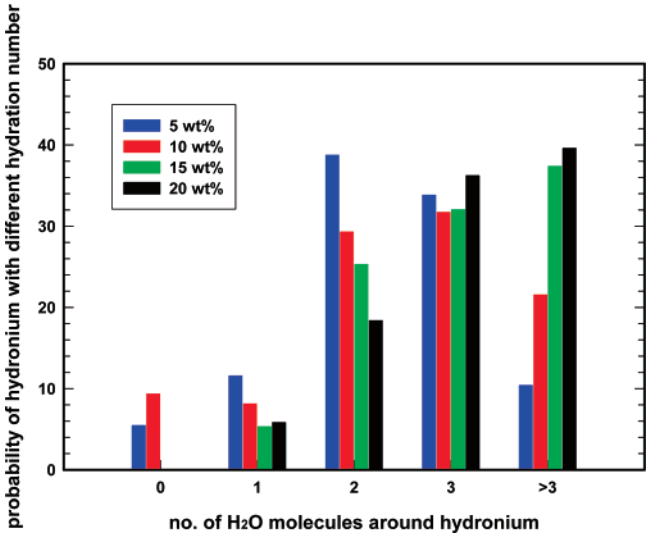

Figure 8. Distribution of water molecules around hydronium ions for all four water contents studied.

We can compare the water structure shown in Figure 5 with work published structures of water on Pt.[34,36] While we do see domains of ordered structure, we do not see the same structure. Given the classical nature of this molecular model, it is not surprising that there are differences between this structure and that provided by density functional theory. However, what these classical simulations do provide is a larger scale picture of the distribution of water, hydronium, and Nafion on the Pt surface. Accepting these differences, we proceed with an analysis of the material on the Pt surface.

The structure of water on the catalyst surface can be quantitatively characterized through a pair correlation function (PCF). In Figure 6, we show the PCF for the oxygen atoms of water with other oxygen atoms of waters (the $O_{H_2O}-O_{H_2O}$ PCF) in the adsorbed region next to the catalyst surface as a function of water content. We define the adsorbed region to extend 10 Å above the catalyst surface. We observe that the range of the structure increases as the water content increases. Compared with previous work,[33] the PCFs show similar profiles, but we find two different behaviors: (i) the four peaks corresponding to the adsorbed water layers adjacent to the catalyst surface are much more enhanced; (ii) when the distance $r > 4$ Å, the PCFs shown in Figure 6 oscillate with distance. In our previous paper,[33] the PCFs of the four water contents varied smoothly, displaying a liquidlike structure. In other words, the water on the platinum surface has an enhanced long-range structure.

In Figure 7, we show the PCFs for the oxygen atoms of water with oxygen atoms of hydronium (the $O_{H_2O}-O_{H_3O^+}$ PCF) in the adsorbed region next to the catalyst surface as a function of water content. We find that the $O_{H_2O}-O_{H_3O^+}$ PCF at the catalyst surface is very similar to the bulk $g(r)$. The PCFs of the four water contents share the same qualitative behavior as that of our previous paper:[33] the first peak occurs at about 2.6 Å, and its height decreases with water content resulting from a decreased binding capacity of hydronium ions to water molecules due to increased humidity. But the height of the PCFs near the platinum surface is enhanced more than that in our previous paper, which means that the degree of hydration (or equivalently, the degree of hydrogen bonding in the system) is enhanced next to the catalyst surface relative to that in the bulk hydrated membrane.

In Figure 8, we present a histogram representing the distribution of the number of water molecules around a hydronium ion

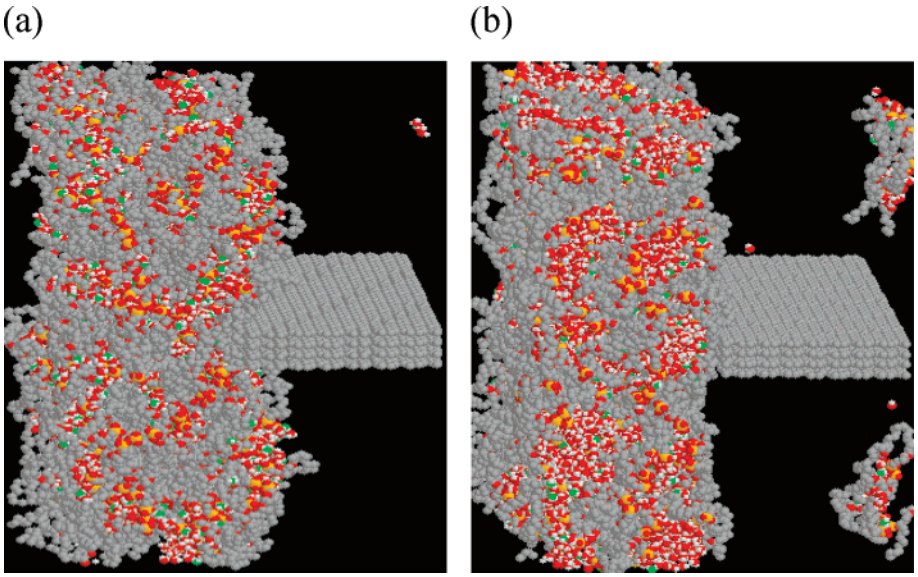

Figure 9. Final snapshots of simulations containing the catalyst support surface for water contents of (a) 5 and (b) 20 wt %. The coloring legend is the same as Figure 2, with the addition that graphitic carbon is gray.

for all four water contents in the absorbed region next to the catalyst surface. In this case, we include all water molecules with the O atom within 3.2 Å of the O of the hydronium ion. The notable feature in this histogram is that the hydration number is shifted to a higher value with the increased water content. We see that hydronium ions adsorbed to the catalyst surface in the 5 wt % water system are most likely bound to two water molecules. For the 10 and 15 wt % systems, the hydroniums are most likely bound to three water molecules, allowing for the possibility of an Eigen ion to form. In the 20 wt % system, the hydronium ion can be bound to more than three water molecules. One can visualize the 4-fold coordination of the hydronium ion at 20 wt % in Figure 5b. We have previously presented these histograms for water in bulk hydrated Nafion.[33]

These PCFs and histograms have implications for proton transport. Proton conductivity occurs via both vehicular diffusion of the hydronium ion and structural diffusion described first by the Grotthuss mechanism[67] and more recently as a fluctuation between states known as Zundel ions ($H_5O_2^+$) and Eigen ions ($H_9O_4^+$); see, for example, refs 68−71. Despite the fact that we use a nonreactive potential, we can still obtain information relevant to the ability of hydronium ions to explore configurations in which they can participate in structural diffusion. The $O_{H_2O}-O_{H_3O^+}$ PCF shown in Figure 7 captures the degree of hydration of the hydronium ion. In bulk water, a hydronium ion must be hydrogen bound to at least three water molecules in order to form an Eigen ion. In quantum mechanical simulations of polymer electrolyte fragments, it has been shown that an oxygen atom of an SO_3^- group at the end of the side chain can participate in structural diffusion by substituting for either one of the oxygen atoms in the Zundel ion or by forming one of the necessary hydrogen bonds in the Eigen ion.[72] Therefore, the hydration of the hydronium ion provides a description of the local environment important for structural diffusion. At the very minimum, hydronium ions that are hydrated by fewer than two water molecules are unlikely to form Eigen ions. Thus, in Figure 8, there is a significant decrease in the fraction of hydronium ions on the Pt surface that are in local environments where they can participate in structural diffusion at lower water contents.

III.B. Membrane/Vapor/Support Systems. Additional simulations were performed that contained the catalyst support surfaces, which we have modeled as graphite. In parts a and b of Figure 9, we present snapshots of the final configuration of the membrane/vapor/support system for hydrated membranes with initial water contents of 5 and 20 wt %, respectively. Again, we observe two surfaces because the simulations are periodic. Notably, there is no wetting of the surface at either water content. We observed no wetting of the graphite surface at 10 and 15 wt % either (not shown here). The failure of water, Nafion, or hydronium ions to adsorb to the graphite surface can be attributed to the fact that the energetic attraction of a graphitic carbon atom is about 80 times weaker than a platinum atom ($\epsilon_C/\epsilon_{Pt} = 0.012$).

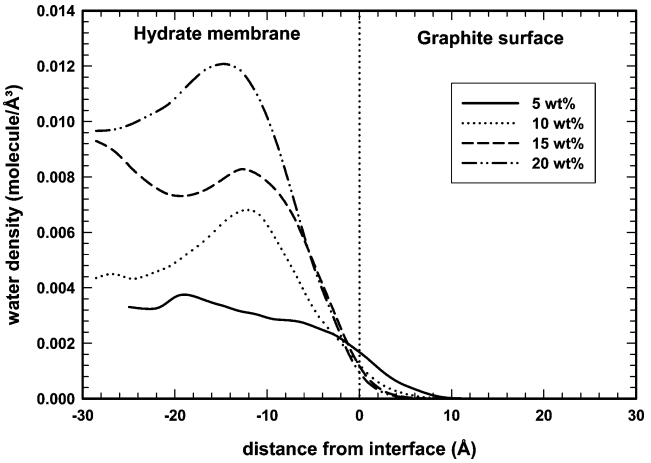

Figure 10. Density profile of water molecules along *z* direction in the simulation cell for the catalyst support system.

The density profile of water in the support system is shown in Figure 10. Again, the zero coordinate on the *x* axis corresponds to the central location of the membrane/vapor interface. The variation of water density within the interface is a consequence of the fact that the nanostructured segregation of the hydrated membrane into hydrophobic and hydrophilic regions is not uniform on the nanoscale and relaxes on a time scale that is greater than the duration of these simulations. As was the case with the catalyst surface, there is clearly a "dehydrated region" of the membrane near the interface. We observe virtually no adsorption of water on the support surface.

IV. Implications and Conclusions

In this work we have studied the molecular-level structure of the electrode/electrolyte interface. We acknowledge that the detail of the electrode−electrolyte environment is a function of the manufacturing procedure, the composition of the MEA, and the operating conditions of the fuel cell. In this work, we have focused on model interfaces that we believe are present in a wide range of MEAs across a range of operating conditions. In this model, the pore contains water vapor.

Regardless of the structure, the catalyst particle must be able to participate in three transport processes: (i) diffusion of molecular hydrogen in a vapor phase to the catalyst surface, (ii) conduction of electrons to the electrode, and (iii) diffusion/conduction of protons to the electrolyte membrane. Each of these three transport properties taken independently has an asymptotic optimal configuration associated with it. Because the diffusivity of a gas is orders of magnitude higher than that of a liquid (at room temperature and pressure, the self-diffusivity of H_2 is 5.6×10^{-1} cm^2/s,[49] and the diffusivity of H_2 in water is 4.5×10^{-5} cm^2/s[50]), the optimal diffusion of molecular hydrogen would occur on a bare electrode (in which none of the surface is coated with thick layers of water or Nafion). The optimal conduction of electrons requires significant and direct contact between all catalyst particles and the conducting component of the electrode. The optimal conduction of protons requires that all catalyst particles have significant and direct contact with electrolyte in the membrane or leading to the membrane. This optimization procedure is constrained by the desire to minimize the amount of catalyst in the MEA.

The optimization of the performance of PEM fuel cells can benefit from atomic and molecular scale level understanding of the various reactive and transport processes occurred at the electrode/electrolyte interface in the system. We have shown that, at higher water contents, the initially bare catalyst surface is likely to be covered by a monolayer which is a mixture of water, Nafion, and hydronium ions. At the anode, the gaseous hydrogen fuel must reach the catalyst surface, penetrating this monolayer. Furthermore, once the electron and proton of the hydrogen atom have been dissociated, the ability of the proton to form a hydronium ion depends upon the availability of water bound to the catalyst surface. If the surface is dry (as much of it appears to be at low water content), then the relevant surface diffusion process is that of the proton. If the surface is wet, then the relevant surface diffusion process is that of the hydronium ion.

We showed that there is virtually no wetting of the support material (graphite in this work). This observation has implications for effective catalyst utilization. In Figure 1, we show two catalyst particles, one immediately adjacent to the polymer electrolyte membrane and one bound to the support but separated by some distance from the membrane. If there is no wetting of the support surface, then there can be no transport of protons (or hydronium ions) across this gap. Therefore, while catalyst particles may be able to adsorb gaseous molecular hydrogen and dissociate it into protons and electrons, if the protons cannot reach the polymer electrolyte membrane, then that catalyst particle cannot contribute to power generation and is ultimately useless. The likelihood of finding a catalyst particle in this state is again a function of the manufacturing process and composition of the MEA. We are currently performing MD simulations to study quantitatively the critical size of the gap between a catalyst particle and the polymer electrolyte membrane across which protons may travel, and the dependence of that critical size on water content.

In conclusion, we performed molecular dynamics simulations of the hydrated polymer electrolyte membrane/vapor/catalyst three-phase interface and the hydrated polymer electrolyte membrane/vapor/support three-phase interface, using Nafion, [100] platinum, and graphite atoms. Characterization and analysis of the configurational and dynamic properties indicate that there is no wetting of the catalyst support surface (graphite in this work) and significant wetting of catalyst surface ([100] platinum in this work). The degree of wetting increases on the catalyst surface with the water content, but we do not observe more than a monolayer on the surface. This monolayer is composed of a mixture of water, Nafion, and hydronium ions. At high water contents, the water forms a regular lattice on the catalyst surface. We characterized the structure of water molecules and hydronium ions adsorbed to the catalyst surface by the PCFs.

There are two main implications of this work. First, fundamental work is required to study the adsorption and dissociation of molecular hydrogen on catalyst surface with adsorbed layers, such as those described herein. Furthermore, the overall diffusion of protons (including vehicular and structural diffusion) across this surface, as a function of water content, must be investigated at a fundamental level, if one is to quantitatively understand the molecular mechanisms for proton transport at the electrode/electrolyte interface. The second implication of this work is that, because the catalyst support shows no significant wetting, the catalyst particles must be in intimate contact with the hydrated membrane, or with recast hydrated polymer electrolyte membrane in the electrode that provides a pathway for protons to move from the catalyst surface into the bulk hydrated membrane. Work is currently underway to study the critical gap size across which protons can be transported.

Acknowledgment. The work is supported by a grant from the U.S. Department of Energy BES under Contract No. DE-FG02-05ER15723. This research used resources of the Center for Computational Sciences at Oak Ridge National Laboratory, which is supported by the Office of Science of the DOE under Contract DE-AC05-00OR22725.

References and Notes

(1) Eisenberg, A. *Macromolecules* **1970**, *3*, 147.
(2) Falk, M. *Can. J. Chem.* **1980**, *58*, 1495.
(3) Roche, E. J.; Pineri, M.; Duplessix, R.; Levelut, A. M. *J. Polymer Sci. B: Polym. Phys.* **1981**, *19*, 1.
(4) Gierke, T. D.; Munn, G. E.; Wilson, F. C. *J. Polymer Sci. B: Polym. Phys.* **1981**, *19*, 1687.
(5) Yeager, H. L.; Steck, A. *J. Electrochem. Soc.* **1981**, *128*, 1880.
(6) Fujimura, M.; Hashimoto, T.; Kawai, H. *Macromolecules* **1981**, *14*, 1309.
(7) Roche, E. J.; Pineri, M.; Duplessix, R.; Levelut, A. M. *J. Polym. Sci. B: Polym. Phys.* **1981**, *19*, 1.
(8) Fujimura, M.; Hashimoto, T.; Kawai, H. *Macromolecules* **1982**, *15*, 136.
(9) Hsu, W. Y.; Gierke, T. D. *J. Membr. Sci.* **1983**, *13*, 307.
(10) Heaney, M. D.; Pellegrino, J. *J. Membr. Sci.* **1989**, *47*, 143.
(11) Verbrugge, M. W.; Hill, R. F. *J. Electrochem. Soc.* **1990**, *137*, 886.
(12) Porat, Z. e.; Fryer, J. R.; Huxham, M.; Rubinstein, I. *J. Phys. Chem.* **1995**, *99*, 4667.
(13) Lehmani, A.; Durand-Vidal, S.; Turq, P. *J. Appl. Polym. Sci.* **1998**, *68*, 503.
(14) Gebel, G. *Polymer* **2000**, *41*, 5829.
(15) James, P. J.; Elliott, J. A.; McMaster, T. J.; Newton, J. M.; Elliott, A. M. S.; Hanna, S.; Miles, M. J. *J. Mater. Sci.* **2000**, *35*, 5111.
(16) James, P. J.; McMaster, T. J.; Newton, J. M.; Miles, M. J. *Polymer* **2000**, *41*, 4223.
(17) Elliott, J. A.; Hanna, S.; Elliott, A. M. S.; Cooley, G. E. *Macromolecules* **2000**, *33*, 4161.
(18) Kreuer, K. D. *J. Membr. Sci.* **2001**, *185*, 29.
(19) Haubold, H.-G.; Vad, T.; Jungbluth, H.; Hiller, P. *Electrochim. Acta* **2001**, *46*, 559.

(20) Rollet, A.-L.; Gebel, G.; Simonin, J.-P.; Turq, P. *J. Polymer Sci. B: Polym. Phys.* **2001**, *39*, 548.
(21) Young, S. K.; Trevino, S. F.; Beck; Tan, N. C. *J. Polymer Sci. B: Polym. Phys.* **2002**, *40*, 387.
(22) Jinnouchi, R.; Okazaki, K. *J. Electrochem. Soc.* **2003**, *150*, E66.
(23) Spohr, E.; Commer, P.; Kornyshev, A. A. *J. Phys. Chem. B* **2002**, *106*, 10560.
(24) Li, T.; Wlaschin, A.; Balbuena, P. B. *Ind. Eng. Chem. Res.* **2001**, *40*, 4789.
(25) Din, X.-D.; Michaelides, E. E. *AIChE J.* **1998**, *44*, 35.
(26) Eikerling, M.; Kornyshev, A. A.; Kuznetsov, A. M.; Ulstrup, J.; Walbran, S. *J. Phys. Chem. B* **2001**, *105*, 3646.
(27) Paddison, S. J.; Zawodzinski, T. A., Jr. *Solid State Ionics* **1998**, *113*−*115*, 333.
(28) Paddison, S. J.; Pratt, L. R.; Zawodzinski, T. A., Jr. *J. New Mater. Electrochem. Sys.* **1999**, *2*, 183.
(29) Paddison, S. J.; Paul, R.; Zawodzinski, T. A., Jr. *J. Electrochem. Soc.* **2000**, *147*, 617.
(30) Paddison, S. J.; Paul, R.; Zawodzinski, T. A., Jr. *J. Chem. Phys.* **2001**, *115*, 7753.
(31) Vishnyakov, A.; Neimark, A. V. *J. Phys. Chem. B* **2000**, *104*, 4471.
(32) Urata, S.; Irisawa, J.; Takada, A.; Shinoda, W.; Tsuzuki, S.; Mikami, M. *J. Phys. Chem. B* **2005**, *109*, 4269.
(33) Cui, S.; Liu, J.; Selvan, M. E.; Keffer, D. J.; Edwards, B. J.; Steele, W. V. *J. Phys. Chem. B* **2007**, *111*, 2208.
(34) Ogasawara, H.; Brena, B.; Nordlund, D.; Nyberg, M.; Pelmenschikov, A.; Pettersson, L. G. M.; Nilsson, A. *Phys. Rev. Lett.* **2002**, *89*, 276102.
(35) Benjamin, I. *Modern Aspects of Electrochemistry* **1997**, *31*, 115.
(36) Rossmeisl, J.; Norskov, J. K.; Taylor, C. D.; Janik, M. J.; Neurock, M. *J. Phys. Chem. B* **2006**, *110*(43), 21833.
(37) Wilson, M. S.; Gottesfeld, S. *J. Appl. Electrochem.* **1992**, *22*, 1.
(38) Broka, K.; Ekdunge, P. *J. Appl. Electrochem.* **1997**, *27*, 117.
(39) Cheng, X.; Yi, B.; Han, M.; J., Z.; Qiao, Y.; Yu, J. *J. Power Sources* **1999**, *79*, 75.
(40) Antolini, E.; Giorgi, L.; Pozio, A.; Passalacqua, E. *J. Power Sources* **1999**, *77*, 136.
(41) Gode, P.; Jaouen, F.; Lindbergh, G.; Lundblad, A.; Sundholm, G. *Electrochim. Acta* **2003**, *48*, 4175.
(42) Lamas, E. J.; Balbuena, P. B. *Electrochim. Acta* **2006**, *51*, 5904.
(43) Vishnyakov, A.; Neimark, A. V. *J. Phys. Chem. B* **2001**, *105*, 7830.
(44) Elliott, J. A.; Hanna, S.; Elliott, A. M. S.; Cooley, G. E. *Phys. Chem. Chem. Phys.* **1999**, *1*, 4855.
(45) Jang, S. S.; Molinero, V.; Cagin, T.; Goddard, W. A., III. *J. Phys. Chem. B* **2004**, *108*, 3149.
(46) Venkatnathan, A.; Devanathan, R.; Dupuis, M. *J. Phys. Chem. B* **2007**, *111*, 7234.
(47) Petersen, M. K.; Voth, G. A. *J. Phys. Chem. B* **2006**, *110*, 18594.
(48) Esai Selvan, M.; Liu, J.; Keffer, D. J.; Cui, S.; Edwards, B. J.; Steele, W. V. *J. Phys. Chem. C* **2007**, in press.
(49) Bird, R. B.; Stewart, W. E.; Lightfoot, E. N. *Transport Phenomena*, 2nd ed.; John Wiley & Sons, Inc.: New York, 2002.
(50) Lide, D. R. *CRC Handbook of Chemistry and Physics*, 71st ed.; Chemical Rubber Publishing Co.: Boca Raton, FL, 1990.
(51) Morris, D. R.; Sun, X. *J. Appl. Polym. Sci.* **1993**, *50*, 1445.
(52) Cui, S. T.; Siepmann, J. I.; Cochran, H. D.; Cummings, P. T. *Fluid Phase Equilib.* **1998**, *146*, 51.
(53) Cannon, W. R.; Pettitt, B. M.; McCammon, J. A. *J. Phys. Chem.* **1994**, *98*, 6225.
(54) Jorgensen, W. L.; Chandrasekhar, J.; Madura, J. D.; Impey, R. W.; Klein, M. L. *J. Chem. Phys.* **1983**, *79*, 926.
(55) Price, D. J.; Brooks, C. L., III. *J. Chem. Phys.* **2004**, *121*, 10096.
(56) Cornell, W. D.; Cieplak, P. B.; Christopher, I.; Gould, I. R.; Merz, K. M., Jr.; Ferguson, D. M.; Spellmeyer, D. C.; Fox, T.; Caldwell, J. W.; Kollman, P. A. *J. Am. Chem. Soc.* **1995**, *117*, 5179.
(57) Wu, G.-W.; Chan, K.-Y. *J. Electroanal. Chem.* **1998**, *450*, 225.
(58) Picaud, S.; Hoang, P. N. M.; Hamad, S.; Mejias, J. A.; Lago, S. *J. Phys. Chem. B* **2004**, *108*, 5410.
(59) Liem, S. Y.; Chan, K.-Y. *Surf. Sci.* **1995**, *328*, 119.
(60) Koh, S. J. A.; Lee, H. P.; Lu, C.; Cheng, Q. H. *Phys. Rev. B* **2005**, *72*, 085414/1.
(61) Hummer, G.; Soumpasis, D. M.; Neumann, M. *Mol. Phys.* **1992**, *77*, 769.
(62) Cui, S. T.; Harris, J. G. *Chem. Eng. Sci.* **1994**, *49*, 2749.
(63) Hoover, W. G. *Phys. Rev. A* **1985**, *31*, 1695.
(64) Nose, S. *Mol. Phys.* **1984**, *52*, 255.
(65) Nose, S. *J. Chem. Phys.* **1984**, *81*, 511.
(66) Tuckerman, M.; Berne, B. J.; Martyna, G. J. *J. Chem. Phys.* **1992**, *97*.
(67) de Grotthuss, C. J. T. *Ann. Chim.* **1806**, *58*, 54.
(68) Tuckerman, M.; Laasonen, K.; Sprik, M.; Parrinello, M. *J. Chem. Phys.* **1995**, *103*, 150.
(69) Tuckerman, M. E.; Marx, D.; Klein, M. L.; Parrinello, M. *Science* **1997**, *275*, 817.
(70) Marx, D.; Tuckerman, M. E.; Parrinello, M. *J. Phys.* **2000**, *12*, A153.
(71) Agmon, N. *Chem. Phys. Lett.* **1995**, *244*, 456.
(72) Paddison, S. J.; Elliott, J. A. *J. Phys. Chem. A* **2005**, *109*, 7583.